Chapter 3: Figure Legends and Figures

Figure legends

Figure 1. *Structure and excitability of MN5*

(A) Expression patterns of C380-GAL4; UAS-mCD8-GFP, Cha-GAL80 in the ventral nerve cord of the adult fly. (A) shows the thoracic neuromeres with expression in the flight motoneurons MN1-5, a ventral unpaired median (VUM) neuron, and about 10 unidentified neurons in each thoracic hemisegment. The locations of the somata of MN1-5 are marked by white arrows. Expression of mCD8-GFP under the control of C380-GAL4 in the abdominal neuromeres is depicted in (Ai). (B) shows the location and overall dendritic structure of the flight motoneurons MN1-5 as revealed by selective retrograde staining from the DLM flight muscle. The fine structure of MN5 is depicted in (C) as a projection view of all confocal optical sections into one image plane. The intracellular label of MN5 is superimposed by a 3-dimensional dendritic reconstruction in (Ci). The run of the link segment is indicated by two white arrows (see text). The branching structure as determined by geometric reconstruction is shown as dendrogram in (Cii). Representative traces from *in situ* patch-clamp recordings from the soma of MN5 in current-clamp mode are shown in (D). Injecting current into the soma of MN5 results in a phasic firing response. The current injection protocol is shown as inset in (D). From the resting membrane potential 14 current injections of 200 ms duration and with increasing amplitude in 100 pA increments were given. The larger the amplitude of the injected current, the shorter is the delay to action potential initiation. This is shown as selective enlargement of the time scale in (Di). (Dii) shows 14 consecutive sweeps of increasing current injection amplitude at a low but easy to compare time resolution. To account for some variability as occurring in the recordings in (E) a non-representative extreme example of a similar current-clamp experiment is shown. The firing response to somatic current injection is also phasic but triplets of spikes occur. (F) shows a representative example of the existence of a sag potential upon negative somatic current injection.

Figure 2. *Intrinsic in vivo excitability of MN5 is altered by genetic manipulations of potassium channels*

Representative examples of spiking responses to current injected into the soma of MN5 as determined by *in situ* patch-clamp recordings are depicted for 4 different genotypes in (A to D). Selective enlargements of the onset of the voltage response to 1.4 nA current injection are

shown in (Ai to Di). The typical phasic firing responses of MN5 from heterozygous control animals is shown in (A). Dominant negative *eag* potassium channel knock-down increases the number of spikes caused by current injections of a given amplitude, but the firing patterns are still phasic, and the amplitude of additional spikes becomes increasingly smaller (B). Dominant negative double knock-down of *eag* and *Shaker* causes a tonic firing response (C). Expression of two copies of EKO causes an absence of action potentials as response to somatic current injection.

To account quantitatively for variability in the firing responses within each genotype, the firing responses were classified in 5 types (no response, graded peak, single spike, phasic firing and tonic firing). The percentage of recordings falling into each of these categories is plotted for each of the four genotypes (E).

Figure 3. *Genetic manipulations of potassium membrane currents do not affect overall but detailed dendritic branching structure*

The left column (A to D) shows representative intracellular stainings of MN5 from different genotypes. For visualization of all dendrites in one image, all optical sections from confocal image stacks are projected into one image plane using the maximum intensity method (A = control; B = *eag*SDN double knock-down; C = *eag*DN knock-down; D = expression of EKO). In (Ai to Di) the projection views are overlaid with images of geometric reconstructions from confocal image stacks. In (Aii to Dii) the branching diagrams (dendrograms) resulting from geometric reconstructions are shown.

Figure 4. *Quantitative comparison of the dendritic structure of MN5 from control, hyperexcitable (eagSDN knock-down) and hypoexcitable (expression EKO) MN5*

The total dendritic length (TDL) from all 3 genotypes is shown in (A). The number of branch points is depicted in (B). Mean dendritic length of all dendritic segments is shown in (C), and the mean maximum branch order for each genotype is depicted in (D). The mean distance of all dendritic segments to the origin of the tree is depicted in (E) and mean surface of all three genotypes is shown in (F). Green bars are control, dark blue bars represent *eag*SDN, and light blue bars are EKO. Error bars represent standard deviation. The number of animals for

*eag*SDN and EKO is 5 each, and the number of control animals is 7. Statistical significance is indicated by asterisks; * = $p < 0.05$, ** = $p < 0.001$.

Figure 5. *Branch order analysis of the dendritic structure of MN5 from control, hyperexcitable (eagSDN knock-down) and hypoexcitable (expression EKO) MN5*

(A) shows the mean number of dendritic branches (y-axis) per branch order. (B) shows the mean dendritic branch length per branch order. Green bars are control, dark blue bars represent *eag*SDN, and light blue bars are EKO. The number of animals for *eag*SDN and EKO is 5 each, and the number of control animals is 7.

Figure 6. *Dendritic diameters are altered in MN5 with EKO mediated decreased intrinsic excitability.*

Mean dendritic diamters (y-axis) are plotted as a function of branching order. Green bars are control and light blue bars represent EKO. Error bars represent standard deviations. Data are from 7 control and 5 EKO reconstructions.

Figure 7. *Genetic manipulations affect flight motor performance.*

(A) Time lapse images of restrained flight behavior show subsequent images of one wing beat filmed at 1000 frames per second. (B) shows the percentage of flies responding with flight motor behavior after tarsal contact with the substrate is terminated and a wind stimulus is applied to the animals head. (C) depicts the median and upper and lower quartiles of the flight duration to the first stop (initial flight). (D) shows the median and upper and lower quartiles of the total flight duration until the flies stopped responding with flight behavior to three consecutive wind stimuli. Green bars are control (n = 37), dark blue bars represent *eag*SDN (n = 38), and light blue bars are EKO (n = 25). Asterisks indicate statistical significance. Mann and Whitney U-test, $p < 0.05$.

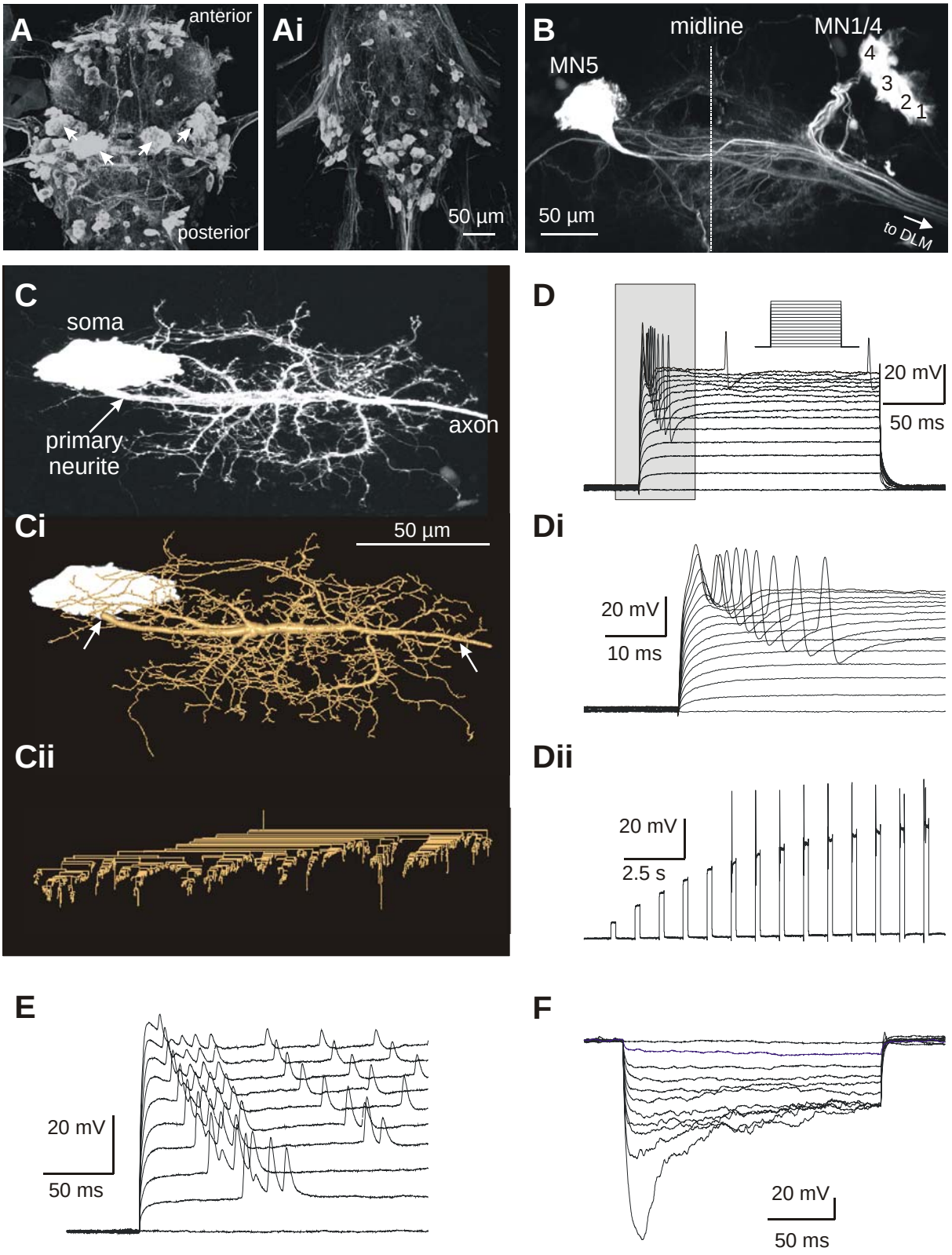
A
anterior
posterior
Ai
50 µm
B
midline
MN1/4
4
3
2
1
MN5
50 µm
to DLM
C
soma
primary neurite
axon
Ci
50 µm
Cii
D
20 mV
50 ms
Di
20 mV
10 ms
Dii
20 mV
2.5 s
E
20 mV
50 ms
F
20 mV
50 ms

figure 1

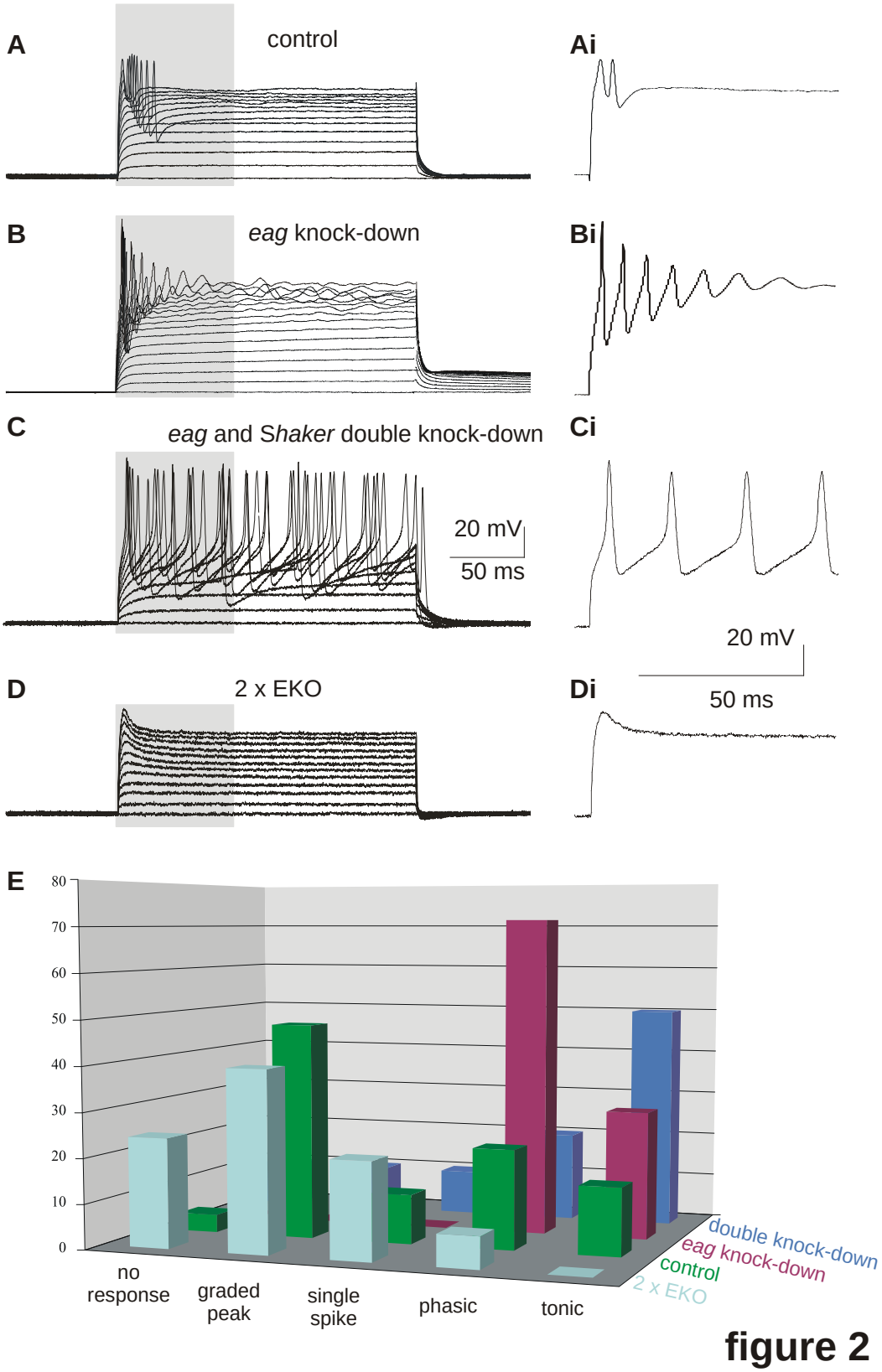
A
control
Ai
B
eag knock-down
Bi
C
eag and Shaker double knock-down
Ci
20 mV
50 ms
20 mV
50 ms
D
2 x EKO
Di
E
80
70
60
50
40
30
20
10
0
no response
graded peak
single spike
phasic
tonic
double knock-down
eag knock-down
control
2 x EKO

figure 2

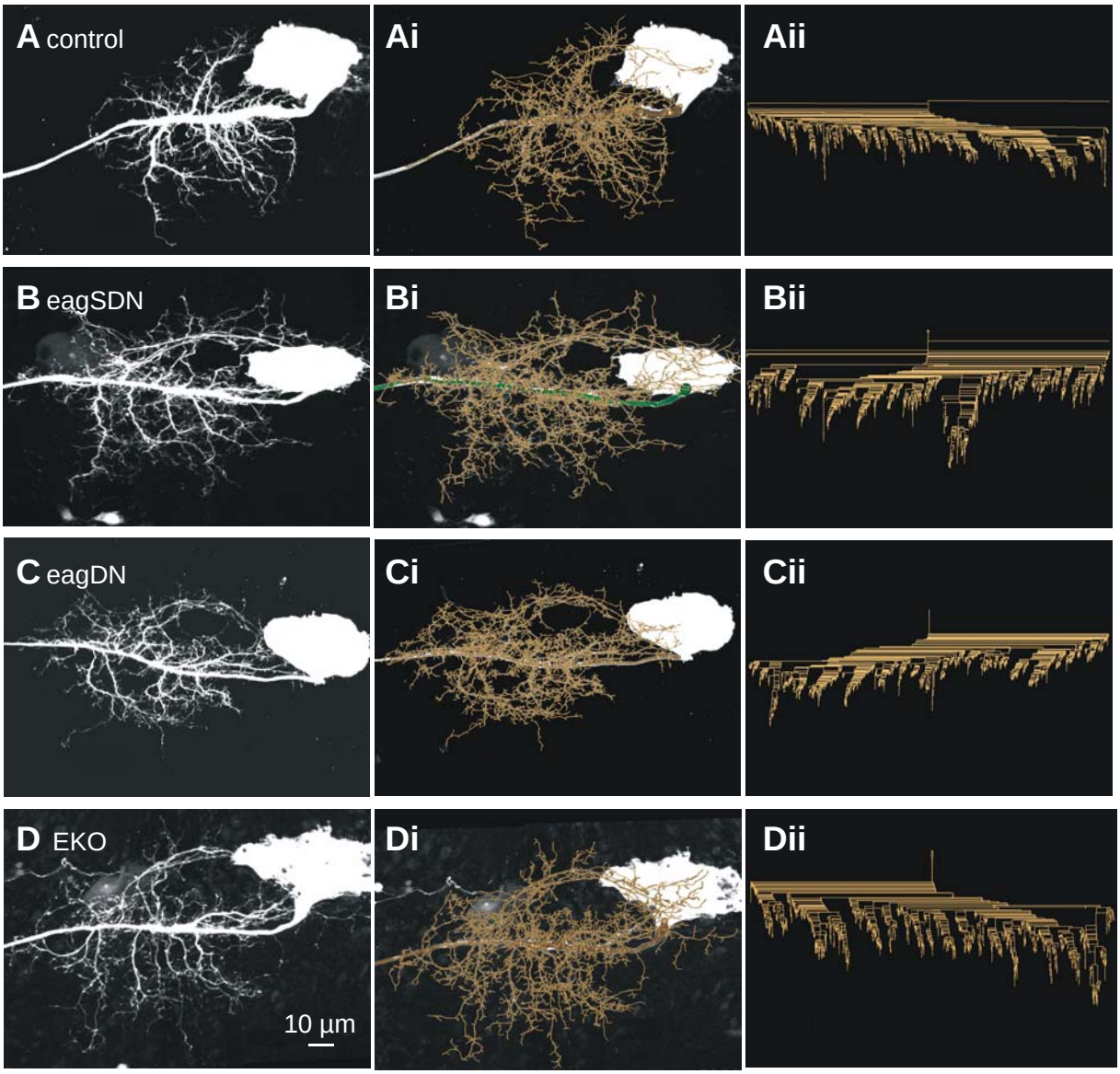

figure 3

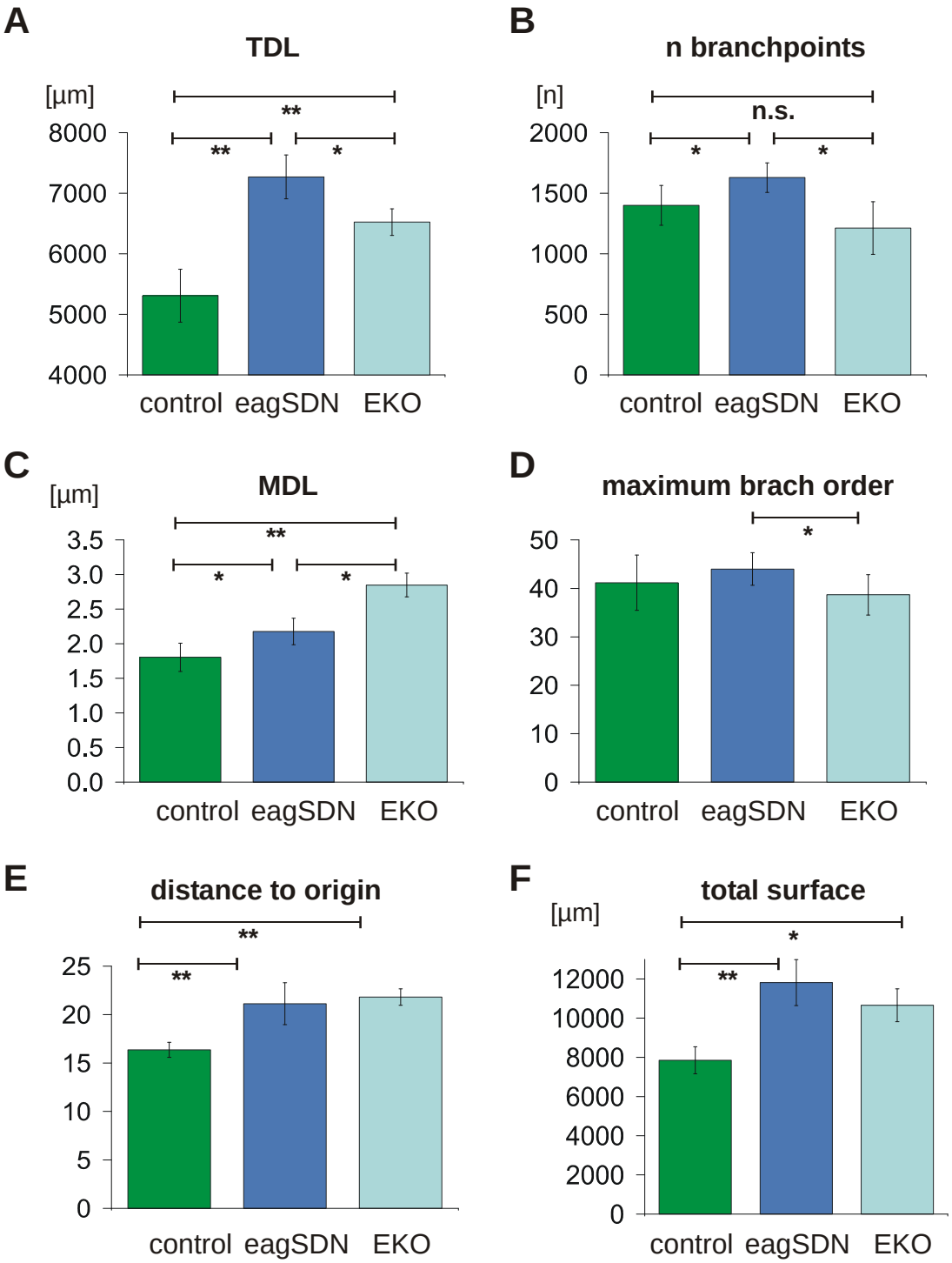
A
TDL
[µm]
8000
7000
6000
5000
4000
**
**
*
control
eagSDN
EKO
B
n branchpoints
[n]
2000
1500
1000
500
0
n.s.
*
*
control
eagSDN
EKO
C
MDL
[µm]
3.5
3.0
2.5
2.0
1.5
1.0
0.5
0.0
**
*
*
control
eagSDN
EKO
D
maximum brach order
50
40
30
20
10
0
*
control
eagSDN
EKO
E
distance to origin
25
20
15
10
5
0
**
**
control
eagSDN
EKO
F
total surface
[µm]
12000
10000
8000
6000
4000
2000
0
*
**
control
eagSDN
EKO

figure 4

A **number of branches per order**

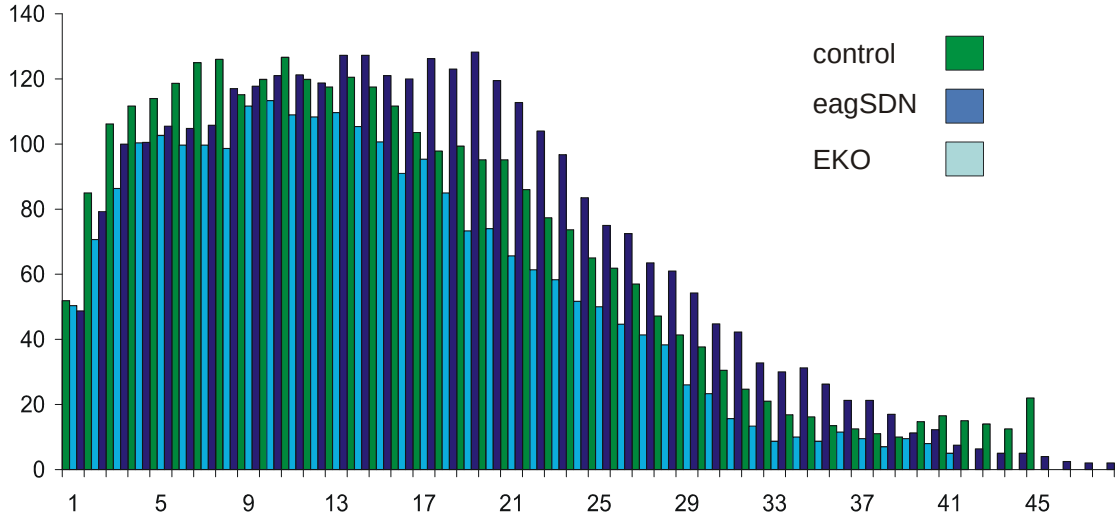

B **mean dendritic branch length per order**

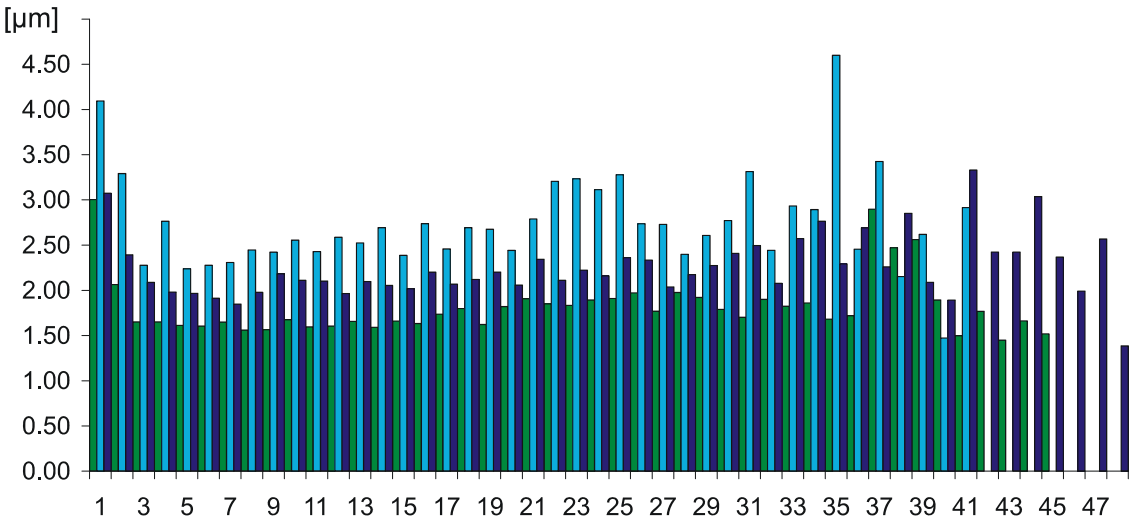

figure 5

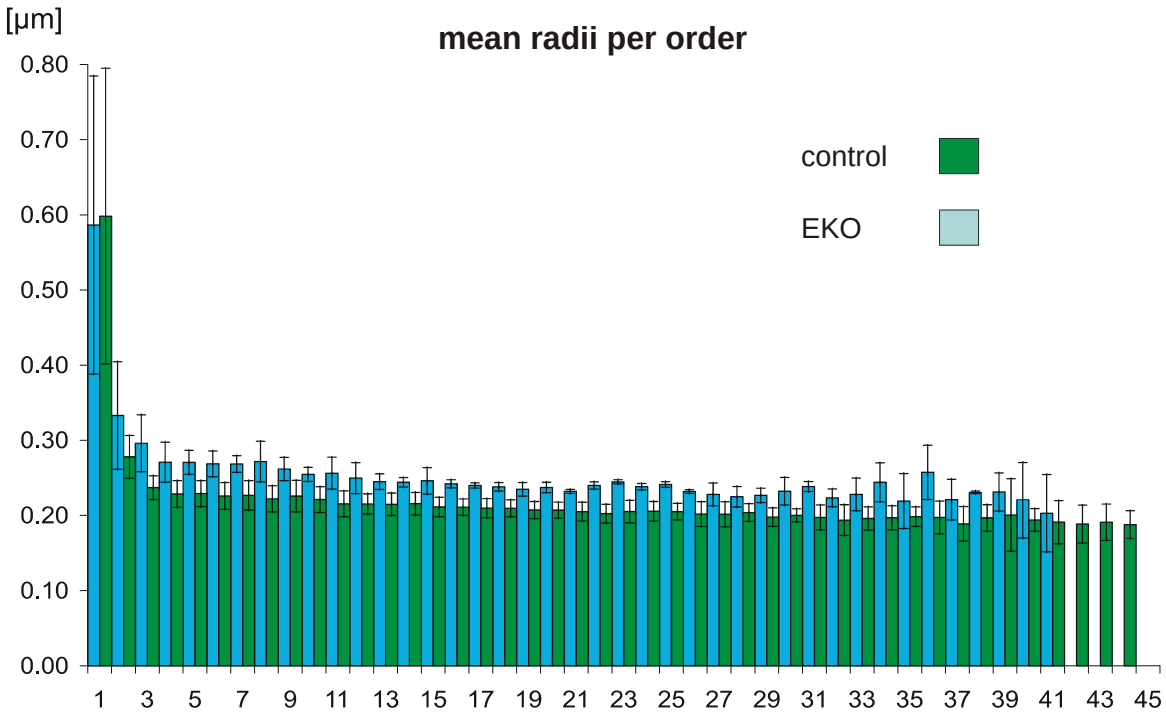
[µm]
mean radii per order
0.80
0.70
0.60
0.50
0.40
0.30
0.20
0.10
0.00
control
EKO
1 3 5 7 9 11 13 15 17 19 21 23 25 27 29 31 33 35 37 39 41 43 45

figure 6

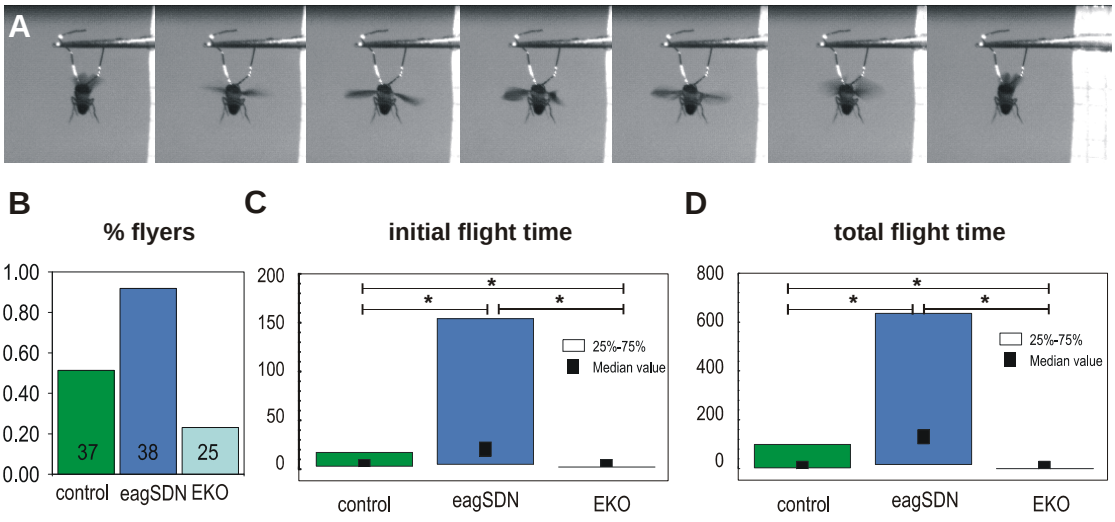
A
B
% flyers
1.00
0.80
0.60
0.40
0.20
0.00
37
38
25
control
eagSDN
EKO
C
initial flight time
200
150
100
50
0
*
*
*
25%-75%
Median value
control
eagSDN
EKO
D
total flight time
800
600
400
200
0
*
*
*
25%-75%
Median value
control
eagSDN
EKO

figure 7